Possibility for exciton Bose-Einstein condensation in carbon nanotubes

I. V. Bondarev[*] and A. V. Meliksetyan

Department of Math & Physics, North Carolina Central University, Durham, North Carolina 27707, USA

We demonstrate a possibility for exciton Bose-Einstein condensation in individual small-diameter ($\sim$1–2 nm) semiconducting carbon nanotubes. The effect occurs under the exciton-interband-plasmon coupling controlled by an external electrostatic field applied perpendicular to the nanotube axis. It requires fields $\sim$1 V/nm and temperatures below 100 K that are experimentally accessible. The effect offers a testing ground for fundamentals of condensed matter physics in one dimension and opens up perspectives to develop tunable coherent polarized light source with carbon nanotubes.

PACS number(s): 78.67.Ch, 73.22.−f, 73.63.Fg, 78.40.Ri

I. INTRODUCTION

Carbon nanotubes (CNs), graphene sheets rolled-up into cylinders of one to a few nanometers in diameter and up to hundreds of microns in length, have been successfully integrated into miniaturized electronic, electromechanical, chemical devices, scanning probes, and into nanocomposite materials [1,2]. Over the past few years, optical nanomaterials research has uncovered intriguing optical attributes of their physical properties lending themselves to a variety of optoelectronic device applications [3–14]. The great breadth and depth of optical phenomena in CNs is exemplified by experimental and theoretical reports on how their optical properties are affected by defects [15–17], exciton-phonon interactions [18–20], biexciton and trion formation [21–28], exciton-plasmon coupling [29], and external magnetic [30] and electric fields [29,31]. Recent studies have also looked at thermal rectification [32], microwave-frequency signal rectification [33], and nonlinear optical response of individual CNs [34]. Several efforts reported on semiconducting CNs used for the generation, detection, and harvesting of light [6–13], and as single photon sources for quantum computing, communication, or cryptography [35–37].

Undoped semiconducting single-wall CNs are direct band-gap semiconductors and feature very large exciton binding energies (hundreds of meV) [4,5]. Excitonic excitations in CNs are very stable, with radiative decay lifetimes ranging from $\sim$10 ps to 10 ns [15,38]. Other typical exciton relaxation times are $\sim$30–100 fs for the exciton-phonon scattering [31], and $\sim$50 ps for the exciton scattering by defects [15,16]. Excitonic characteristics in CNs can be adjusted in controllable ways, in order to modify their underlying optical properties. This offers new functionality and creates a strong potential for future tunable optoelectronic device applications with CNs.

Excitons in pristine CNs can be affected by either electrostatic doping [9,39] or by the quantum confined Stark effect (QCSE) [12,29] (an external electrostatic field applied perpendicular to the CN axis; the effect is used recently to tune the band gap of bilayer graphene [40]). In both cases, exciton properties are mediated by collective plasmon excitations. QCSE, in particular, allows one to control exciton-interband-plasmon coupling in individual undoped CNs and their (linear

[12,13,29] and nonlinear [23,41]) optical absorption [42]. Plasmons cannot be excited by light in optical absorption since they are longitudinal excitations while photons are transverse [43,44]. In small-diameter ($\sim$1 nm) semiconducting CNs, light polarized along the CN axis excites excitons [45], which can then couple to the nearest (same-band) interband plasmons [29]. Both of these collective excitations come from the same electronic transitions and, therefore, occur at the same energies $\sim$1 eV, as opposed to bulk semiconductors where they are separated by tens of eVs [43]. They do have different physical nature. Their coexistence at the same energies in CNs is a unique general feature of confined quasi-one-dimensional (1D) systems where the transverse electronic motion is quantized to form 1D bands and the longitudinal one is continuous.

The formation of coupled exciton-plasmon excitations can be viewed as an additional nonradiative channel (in addition to phonons [18,19] and defects [15,16]) for the exciton relaxation in CNs, whereby optically excited excitons decay into low-energy interband plasmons [12,13]. In so doing, excitons generate the quanta of plasma oscillations on the CN surface, on the one hand, and this shortens their lifetime, on the other. Thus, by varying the exciton-plasmon coupling strength with the QCSE one controls both the radiative exciton emission and nonradiative exciton-to-plasmon energy transfer. This latter phenomenon is similar to the SPASER effect (surface plasmon amplification by stimulated emission of radiation) reported earlier for hybrid metal-semiconductor-dielectric nanostructures [46]. It takes place in *individual* small-diameter CNs though, resulting in new strongly coupled hybridized excitations—exciton-plasmons—and associated high-intensity coherent oscillating fields concentrated locally along the CN surface [12,13]. These near fields can be used in a variety of new optoelectronic applications, including near-field nonlinear-optical probing and sensing, optical switching, enhanced electromagnetic absorption, and materials nanoscale modification.

Apart from applications, carbon nanotubes offer an ideal testing ground to study the fundamentals of condensed matter physics in one dimension. Here, in particular, we discuss a possibility for the 1D Bose-Einstein condensation (BEC) phenomenon that originates from the strong coupling of excitons and same-band interband plasmons enabled by using the QCSE. Indeed, exciton-plasmons in an individual nanotube are strongly correlated collective Bose excitations and, therefore, could likely be condensed under appropriate

———————
[*]Corresponding author: ibondarev@nccu.edu

external conditions—in spite of the well-known statements of the BEC impossibility in ideal 1D/2D systems [47] and experimental evidence for no exciton BEC effect in highly excited semiconducting CNs [48]. Possibilities for achieving BEC in 1D and 2D systems are theoretically demonstrated in the presence of an extra confinement potential [49]. We show that the strongly correlated exciton-plasmon system in a CN in a perpendicular electrostatic field presents such a special case. We find the critical BEC temperature, as well as the condensate fraction and its exciton contribution as functions of temperature and electrostatic field applied. We discuss how the effect can be observed experimentally.

Section II briefly reviews the properties of exciton-plasmons in individual small-diameter (∼1–2 nm) semiconducting carbon nanotubes, presents their dispersion relation as a function of the exciton longitudinal momentum and the perpendicular electrostatic field applied, and gives a qualitative reasoning of why the exciton-plasmon BEC effect is possible. Section III develops the theory of the effect and discusses our calculations for the critical BEC temperature, the exciton-plasmon condensate fraction, and its exciton contribution. Section IV summarizes our results and sets forth our vision of how the effect can be investigated experimentally, as well as prospective avenues it challenges for future experimental nanoplasmonics and near-field optics research development, currently focused mostly on metallic nanoparticles [50,51], to include a new area of nanotube plasmonics. Technical details of the theory and derivations are presented in Appendices A and B in order not to interrupt the flow of arguments and results.

II. DISPERSION OF EXCITON-PLASMONS

In small-diameter semiconducting carbon nanotubes, because of their quasi-one-dimensionality, excitons are excited by the external electromagnetic (EM) radiation polarized along the CN axis [45]. [We use the cylindrical coordinate system, Fig. 2(a), with the z axis being the CN symmetry axis.] As a consequence, the exciton quasimomentum vector and transition dipole moment operator are both directed predominantly along the CN axis (the longitudinal exciton). This prevents the exciton from the electric dipole coupling to transversely polarized surface EM modes of the nanotube, those originating from the EM vector potential due to the relative motion of electrons and nuclei on the CN surface, as they propagate predominantly along the CN axis with their electric vectors orthogonal to the propagation direction. Longitudinally polarized surface EM modes originate from the EM scalar potential (see, e.g., Ref. [52]) due to the relative motion of electrons and nuclei, and thus represent CN surface plasmon excitations. These have their electric vectors directed along the propagation direction, and therefore can couple to longitudinal excitons on the CN surface [29]. Experimental evidence for such plasmon modes in CNs was first reported in Ref. [53]. They occur both at high energies (well-known π plasmon at ∼6 eV) and at comparatively low energies of ∼0.5–2 eV. The latter ones are related to the circumferentially quantized interband electronic transitions. These are low-energy weakly dispersive plasmon modes [53,54] that are similar to the intersubband plasmons in quantum wells [55]. They occur in the same energy range of ∼1 eV, where

the exciton excitation energies are located in small-diameter (≲1 nm) semiconducting CNs [38,56]. Such low-energy longitudinally polarized surface EM modes can be viewed as charged plasma oscillations created by *standing* charge density waves due to the periodic opposite-phase displacements of the electron shells with respect to the ion cores in the neighboring elementary cells on the nanotube surface [12,13]. In what follows we focus our consideration on the exciton interactions with these particular surface plasmon modes.

The dispersion relation of the coupled exciton-plasmon excitation of branch μ (= 1,2) with energy $\hbar\omega_\mu(\mathbf{k})$ and quasimomentum $\mathbf{k} = \{k_\varphi, k_z\}$, where k_φ is (circumferentially) quantized and k_z is continuous, can be obtained by means of the diagonalization of the total Hamiltonian of interacting excitons and plasmons. Details of the procedure can be found in Ref. [29]. The procedure results in the following dimensionless dispersion equation:

$$x_\mu^2 - \varepsilon_f^2 - \varepsilon_f \frac{2}{\pi} \int_0^\infty dx \, \frac{x \, \bar{\Gamma}_0^f(x)\rho(x)}{x_\mu^2 - x^2} = 0, \qquad (1)$$

where

$$x = \frac{\hbar\omega}{2\gamma_0}, \quad x_\mu = \frac{\hbar\omega_\mu(\mathbf{k})}{2\gamma_0}, \quad \varepsilon_f = \frac{E_f(\mathbf{k})}{2\gamma_0}, \qquad (2)$$

with $\gamma_0 = 2.7$ eV being the carbon-carbon nearest neighbor overlap integral. The exciton total energy in Eq. (2) is of the form

$$E_f(\mathbf{k}) = E_{\text{exc}}^{(f)}(k_\varphi) + \frac{\hbar^2 k_z^2}{2M_{\text{ex}}(k_\varphi)}. \qquad (3)$$

In this equation, the first term represents the excitation energy $E_{\text{exc}}^{(f)}(k_\varphi) = E_g(k_\varphi) + E_b^{(f)}(k_\varphi)$ of the f-internal-state exciton with the (negative) binding energy $E_b^{(f)}$, which is excited on the nanotube surface by the external EM radiation polarized along the CN axis via the interband electric dipole transition $d_z^f = \sum_{\mathbf{n}} \langle 0|(\hat{\mathbf{d}}_{\mathbf{n}})_z|f\rangle$ (summation over lattice sites) with the band gap E_g. The second term stands for the kinetic energy of the translational longitudinal movement of the exciton with the effective mass $M_{\text{ex}} = m_e + m_h$, where m_e and m_h are the (subband-dependent) electron and hole effective masses, respectively. The function

$$\bar{\Gamma}_0^f(x) = \frac{4|d_z^f|^2 x^3}{3\hbar c^3}\left(\frac{2\gamma_0}{\hbar}\right)^2 \qquad (4)$$

is the dimensionless spontaneous decay rate associated with the exciton radiative recombination and

$$\rho(x) = \frac{3S_0}{16\pi\alpha_{\text{FS}}R_{\text{CN}}^2}\text{Re}\frac{1}{\bar{\sigma}_{zz}(x)} \qquad (5)$$

is the surface plasmon density of states (DOS) responsible for the exciton decay rate variation due to its coupling to plasmons. Here $S_0 = (3\sqrt{3}/4)b^2$ with $b = 1.42$ Å being the carbon-carbon interatomic distance, $\alpha_{\text{FS}} = e^2/\hbar c$ is the fine-structure constant, R_{CN} stands for the CN radius, and $\bar{\sigma}_{zz} = 2\pi\hbar\sigma_{zz}/e^2$ represents the dimensionless surface axial conductivity of the nanotube.

Only the axial conductivity σ_{zz} matters in our case here, while the azimuthal one $\sigma_{\varphi\varphi}$ can be neglected being strongly suppressed due to the CN quasi-one-dimensionality and associated transverse depolarization effect [57–60], which is
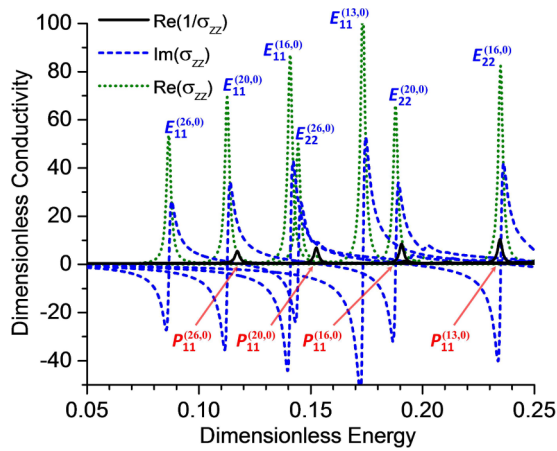
FIG. 1. (Color online) Calculated energy dependence of the dimensionless (normalized by $e^2/2\pi\hbar$) axial surface conductivity σ_{zz} for the four zigzag nanotubes, (13,0), (16,0), (20,0) and (26,0), of increasing diameters. Peaks of $\mathrm{Re}\,\sigma_{zz}$ represent excitons (E_{11}, E_{22}); peaks of $\mathrm{Re}(1/\sigma_{zz})$ represent interband plasmons (P_{11}, P_{22}). Dimensionless energy is defined as [Energy]$/2\gamma_0$, where $\gamma_0 = 2.7$ eV is the C-C overlap integral.

precisely why excitons in small-diameter CNs are excited by light polarized along the CN axis [45,61]. The conductivity factor in Eq. (5) equals

$$\mathrm{Re}\frac{1}{\bar{\sigma}_{zz}(x)} = -\frac{4\alpha_{\mathrm{FS}}c}{R_{\mathrm{CN}}}\left(\frac{\hbar}{2\gamma_0 x}\right)\mathrm{Im}\frac{1}{\epsilon_{zz}(x)-1}$$

in view of Eq. (2) and the Drude relation for nanotubes $\sigma_{zz} = -i\omega(\epsilon_{zz}-1)/4\pi S\rho_T$, where ϵ_{zz} is the longitudinal (along the CN axis) dielectric function, and S and ρ_T are the surface area of the tubule and the number of tubules per unit volume, respectively [58,62–64]. This relates very closely the surface plasmon DOS function (5) to the loss function $-\mathrm{Im}(1/\epsilon)$ measured in electron energy loss spectroscopy (EELS) experiments to study the properties of collective electronic excitations in solids [43,44,53].

Figure 1 shows our calculations of $\bar{\sigma}_{zz}(x)$ for a set of representative zigzag-type semiconducting CNs, (13,0), (16,0), (20,0) and (26,0), of increasing diameters in the range $\sim$1–2 nm ($R_{\mathrm{CN}} = 0.51$, 0.63, 0.78, and 1.02 nm, respectively). We used the ($\mathbf{k}\cdot\mathbf{p}$) method of Ref. [45] with the exciton relaxation time 100 fs for all four CNs (consistent with previous estimates [20,31]). Many-particle Coulomb correlations are included by solving the Bethe-Salpeter equation in the momentum space within the screened Hartree-Fock approximation as described in Ref. [45]. Real conductivities consist of series of peaks ($E_{11}, E_{22}, \ldots$) representing the first, second, etc. excitons. Imaginary conductivities are linked with the real ones by the Kramers-Kronig relation, which is why the functions $\mathrm{Re}(1/\bar{\sigma}_{zz}) = \mathrm{Re}(\bar{\sigma}_{zz})/\{[\mathrm{Re}(\bar{\sigma}_{zz})]^2 + [\mathrm{Im}(\bar{\sigma}_{zz})]^2\}$ show the resonances $P_{11}, P_{22}, \ldots$ right next to $E_{11}, E_{22}, \ldots$. These are the interband plasmon resonances we discussed above (first observed in Ref. [53]). They occur at those (low) energies where the two conditions $\mathrm{Im}[\bar{\sigma}_{zz}(x)] = 0$ and $\mathrm{Re}[\bar{\sigma}_{zz}(x)] \to 0$ are fulfilled simultaneously.

The formation of the strongly coupled hybridized exciton-plasmon excitations is only possible if the exciton total energy
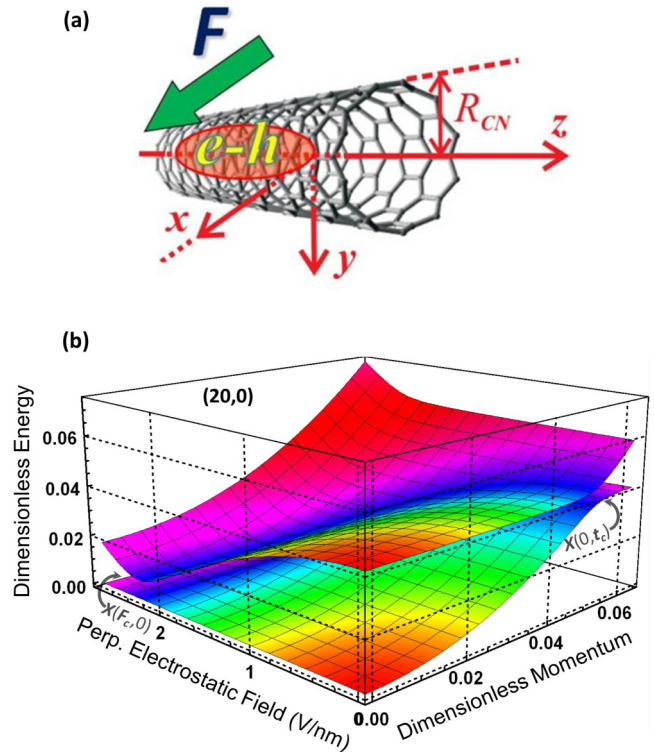
FIG. 2. (Color online) (a) The geometry of the problem. (b) Exciton-plasmon dispersion as a function of the perpendicular electrostatic field and longitudinal momentum for the lowest bright exciton coupled to the nearest interband plasmon in the (20,0) nanotube ($E_{11}^{(20,0)}$ and $P_{11}^{(20,0)}$ in Fig. 1). See text for dimensionless momentum.

is in resonance with the energy of the neighboring (same-band) interband plasmon mode. This can be achieved by using the QCSE with the external electrostatic field F applied perpendicular to the CN axis [Fig. 2(a)]. This problem was first analyzed in Ref. [29], and the effect is shown to be the strongest for the first exciton and the first interband plasmon (E_{11} and P_{11} in Fig. 1). We consider this particular case in what follows.

Perpendicular electrostatic field mixes exciton and plasmon excitations, to result in two branches ($\mu = 1, 2$) of new hybridized quasiparticle states—exciton-plasmons, the solutions to the dispersion equation (1)—with the energies (see Ref. [29])

$$x_{1,2} = \sqrt{\frac{\varepsilon_f^2 + x_p^2}{2} \pm \frac{1}{2}\sqrt{(\varepsilon_f^2 - x_p^2)^2 + (2X_f)^2\varepsilon_f x_p}}, \quad (6)$$

where ε_f [defined in Eq. (2)] and $x_p (= E_p/2\gamma_0)$ are the dimensionless energies of the f-internal-state exciton and interband plasmon of the same band, respectively, $X_f = [2\Delta x_p \bar{\Gamma}_0^f(x_p)\rho(x_p)]^{1/2}$ is the exciton-plasmon Rabi splitting taken at energy $x = x_p$ with $\bar{\Gamma}_0^f(x)$ of Eq. (4), and $\rho(x) \approx \rho(x_p)\Delta x_p^2/[(x-x_p)^2 + \Delta x_p^2]$ is the Lorentzian approximated (of half-width at half-maximum Δx_p proportional to the inverse plasmon lifetime) plasmon DOS function of Eq. (5).

Figure 2(b) shows an example of the two exciton-plasmon branches given by Eq. (6) as functions of the perpendicular

electrostatic field F and longitudinal momentum for the lowest bright ground-internal-state exciton (in which case we drop the f subscript in what follows) coupled to the nearest interband plasmon in the (20,0) nanotube [$E_{11}^{(20,0)}$ and $P_{11}^{(20,0)}$ in Fig. 1]. The origin of the energy is taken to be $x_2(F, k_z = 0)$. In nonzero field $F_c \approx 2$ V/nm, where the strong exciton-plasmon coupling occurs, the upper-branch x_1 has the global minimum at zero momentum, $k_z^c = k_z(F_c) = 0$, separated from the lower branch by the Rabi-splitting $X(F_c, 0) = X(F_c)$. Hence, at equilibrium, if the temperature T is such that $k_B T / 2\gamma_0 > X(F_c)$, strongly coupled upper-branch exciton-plasmons will be distributed around this minimum in the momentum space. Lowering T to get $k_B T / 2\gamma_0 < X(F_c)$ will push them all down to occupy the lowest possible energy state, the $k_z = 0$ state, which is nothing but the exciton-plasmon BEC effect. This effect does not depend on the density of particles though, as opposed to the BEC of noninteracting massive bosons [47,65]. Rather, this is the characteristic feature of the quasiparticle energy spectrum, its dependence on the electrostatic field applied, to be exact, of the coupled exciton-plasmon excitations. Therefore, this BEC effect is hardly sensitive to the interaction, if any, between exciton-plasmons in our system.

Note that the existence of the two equivalent energy valleys in the first Brillouin zone, the K and K' valleys with opposite electron helicities about the CN axis, results in the dark and bright excitonic states in the lowest-energy spin-singlet manifold [4,5,66]. However, since the electrostatic field interaction does not involve spin variables, both K and K' valleys are affected equally by the perpendicular electrostatic field, and so the detailed structure of the exciton multiplet does not manifest itself in our case. This is opposite to the magnetostatic field effect where the field affects the K and K' valleys differently either to brighten the dark excitonic states [30], or to create Landau sublevels [45] for the longitudinal and perpendicular orientations, respectively.

III. EXCITON BEC EFFECT

It is not difficult to derive the BEC fraction as a function of T and F. At $k_z \sim k_z^c = 0$, wherein $\varepsilon_f \sim x_p$, Eq. (6) expands into $x_1(F, s, t) \approx X_f(F, s) + \alpha(s) t^2 / 2$, with the energy counted from $x_2(F, s, t = 0)$, $t = k_z / \tilde{k}_z$ being the dimensionless longitudinal quasimomentum ($|t| \leqslant 1$) and $\alpha = \hbar^2 \tilde{k}_z^2 / 2M_{ex}(s)$. The first Brillouin zone of the CN of (m,n) type ($n \leqslant m$) is taken to be consisting of m parallel lines, as per quantized $k_\varphi = k_\varphi(s) = s / R_{CN}$ with $s = 1, 2, \ldots, m$ and $R_{CN} = (\sqrt{3} b / 2\pi) \sqrt{m^2 + mn + n^2}$, each of length $2\tilde{k}_z = 2B / k_\varphi(m)$, where $2B = 2(4\pi^2 / 3\sqrt{3} b^2)$ is the rectangular area of the reciprocal space covered by the lines, $b (= 1.42$ Å$)$ is the C-C interatomic distance [12]. To obtain the upper-branch exciton-plasmon mean BEC population fraction $\langle n_{10} \rangle$, we use this x_1 and employ the conventional technique (e.g., Refs. [47,65]) to perform the summation over **k** in the first Brillouin zone. For the ground-internal-state exciton, assuming $M_{ex}(s) \approx M_{ex}$ and $X_f(F, s) \approx X(F)$, this results in (see Appendix A for details)

$$\langle n_{10} \rangle (T \leqslant T_c, F) \approx 1 - \frac{T}{T_c(F)}, \qquad (7)$$
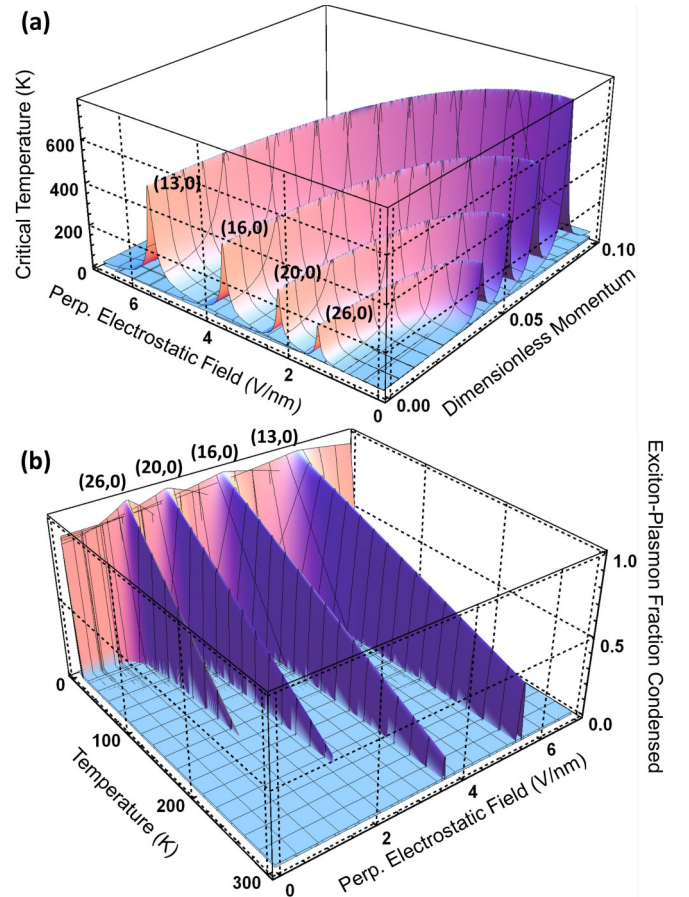
FIG. 3. (Color online) Critical temperatures (a) as functions of the perpendicular electrostatic field applied and longitudinal momentum, and mean upper-branch BEC population fractions (b) as given by Eq. (7), for the four CNs under consideration. See text for dimensionless momentum.

where $T_c(F) = 2\gamma_0 X(F) / k_B$ is the critical temperature with $X(F) = \{2\Delta x_p \bar{\Gamma}_0[\varepsilon(F, t = 0)] \rho[\varepsilon(F, t = 0)]\}^{1/2}$ standing for the exciton-plasmon Rabi splitting at the (excitation) energy of the zero-momentum ground-state exciton. This latter one controls the convergence of the result.

Figure 3(a) shows calculated T_c as functions of F and t (to better understand the general behavior), for the lowest bright ground-internal-state excitons coupled to the nearest interband plasmons in the four CNs under consideration. The functions $T_c(F, t)$ are resonance shaped of widths $\sim 2\Delta x_p$, peaked at $\varepsilon(F, t) \approx x_p(F)$. As F increases, the peak positions shift down to $t \sim 0$, yielding field dependent, resonance shaped $T_c(F)$, same as $X(F)$, peaked at $F_c \sim 1$–6 V/nm with maximum $T_c \sim$ 150–500 K and greater F_c and T_c for smaller diameter CNs. Figure 3(b) presents $\langle n_{10} \rangle$ as given by Eq. (7) for the same case. The quantities $\langle n_{10} \rangle$ reflect the behavior of $T_c(F)$, showing finite BEC fractions throughout the finite ranges of F centered about F_c, expanding in F as T decreases.

Following the general theory of the exciton-plasmon interactions in individual CNs [29], one can now calculate the exciton participation rate in the exciton-plasmon BEC population fraction (7). This is represented by the absolute value squared of the ratio of the exciton mixing coefficient
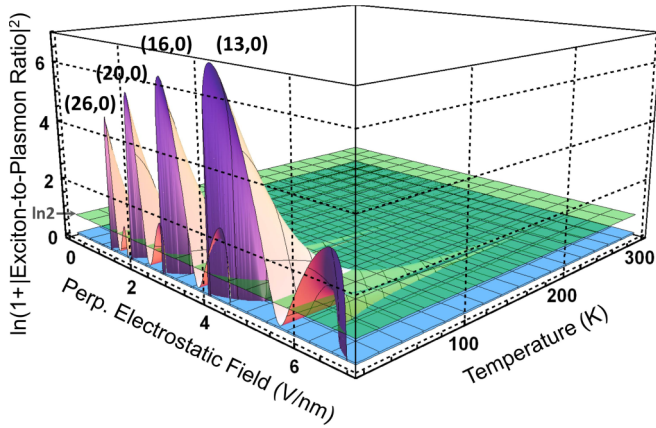
FIG. 4. (Color online) Function $\ln[1 + \langle n_{10} \rangle_{E/P}(0,T,F)]$ calculated using Eqs. (7) and (8) for the CNs under consideration.

to the plasmon mixing coefficient of the upper exciton-plasmon branch. Using the mixing coefficients of Ref. [29] yields thus defined exciton participation rate as a function of dimensionless energy x, T, and F as follows (Appendix B):

$$\langle n_{10} \rangle_{E/P}(x,T,F) \approx \frac{\pi \Delta x_p (x - x_1)^2 (1 + x_1/\varepsilon)^2}{X^2(F)} \langle n_{10} \rangle, \quad (8)$$

with energies to be counted from $x_2(F,t=0)$. Comparing this with Fig. 2(b), we see that at $x = 0$ corresponding to the first ground-state-exciton excitation energy and $F = F_c$ [resonance condition yielding $x_1 = X(F_c)$ and $\varepsilon = X(F_c)/2$], Eq. (8) becomes $9\pi \Delta x_p \langle n_{10} \rangle \ll 1$, meaning that the exciton-plasmon BEC is dominated by plasmons. This is consistent with the coherent plasmon generation effect by excitons reported lately [12,13]. A slight detuning from F_c increases x_1 and dramatically decreases $X(F)$ [Fig. 3(a)], bringing about bursts of $\langle n_{10} \rangle_{E/P} \gg 1$, making the exciton-plasmon BEC dominated by excitons.

The exciton BEC effect is shown in Fig. 4 for the CNs under consideration. It occurs at $F \gtrsim 1$ V/nm and $T \lesssim 100$ K that are experimentally accessible [40]. The effect is stronger and covers broader range of F and T in smaller diameter CNs. Off-resonance coupling to interband plasmons, which are just *standing* charge density waves, slows excitons down by pushing them into periodic effective potential "traps", thereby increasing zero-momentum exciton state population. This is consistent with earlier studies where the 1D/2D BEC phenomenon, otherwise prohibited [47,67,68], is shown to occur in the presence of an extra confinement potential [49].

IV. CONCLUSIONS

The effect of the exciton BEC presented here will manifest itself as highly coherent, longitudinally polarized, far-field exciton emission appearing at temperatures below 100 K as one smoothly increases the perpendicular field strength. Narrow BEC emission peak will be blue shifted by the Rabi-splitting energy from the first exciton excitation energy which the CN should be pumped at by an external laser source. The phenomenon can be investigated in experiments similar to those used for exciton-polariton BEC studies in semiconductor microcavities [69].

To summarize, we have demonstrated theoretically an intriguing possibility for the exciton BEC effect observation in individual semiconducting carbon nanotubes. The quantum system considered here is conceptually similar to the microcavity exciton-polariton system, which started as a theoretical concept in the 1990s and has been a driving force for the experimental physics of low-dimensional semiconductors over the last two decades, exhibiting both new fundamental quantum effects and attractive applications such as polariton lasers, optical polarization switches, superfluid spintronic devices, etc [70]. We, therefore, strongly believe that the quasi-1D exciton BEC effect predicted here not only offers an ideal testing ground for fundamentals of condensed matter physics in one dimension, but also opens up new horizons for a variety of CN based applications ranging from controlled electromagnetic absorption and tunable highly coherent polarized light emission, in particular, to the extension of nanoplasmonics and near-field optics research, currently focused on metallic nanoparticles [50,51], to include a new area of nanotube plasmonics. Further new avenues for experimental nanotube plasmonics research could potentially emerge from the measurements of the coherent BEC exciton emission predicted here if experiments will show that the origin of the emission spot can be translated at will by applying, say, a temperature gradient along the nanotube. Then, a new fundamental effect, the superfluidity of quasi-1D exciton-plasmons in individual CNs, would become a hot research topic for the future. We strongly believe this is only the beginning of nanotube plasmonics as a new research field. Physical understanding of 1D nanophotonics phenomena will greatly benefit from studies of the model system considered herein.

APPENDIX A: DERIVATION OF EQ. (7)

We assume our system as being under constant illumination by low-intensity external monochromatic radiation polarized along the CN axis. This excites excitons and not plasmons since plasmons are longitudinal excitations while photons are transverse [43,44]. Under an applied perpendicular electrostatic field, excitons couple to the nearest (same-band) interband plasmons to form new hybridized excitations—exciton-plasmons [12,13,29], whose occupation numbers, by virtue of the linear response theory in the exciton-radiation interaction and the corresponding fluctuation dissipation theorem [65], can be found as an equilibrium statistical average of the form

$$\langle n_\mu(\mathbf{k}) \rangle = \text{Tr}\left[\frac{e^{-\beta \hat{H}}}{Q} \hat{\xi}_\mu^\dagger(\mathbf{k}) \hat{\xi}_\mu(\mathbf{k}) \right]. \quad (A1)$$

Here $\hat{\xi}_\mu^\dagger(\mathbf{k})$ and $\hat{\xi}_\mu(\mathbf{k})$ create and annihilate, respectively, the exciton-plasmon excitation of branch μ (=1,2) with the momentum $\mathbf{k}$, $\hat{H} = \sum_{\mathbf{k},\mu=1,2} \hbar \omega_\mu(\mathbf{k}) \hat{\xi}_\mu^\dagger(\mathbf{k}) \hat{\xi}_\mu(\mathbf{k})$ is the total Hamiltonian diagonalized of the interacting excitons and

plasmons, and $\hbar\omega_\mu(\mathbf{k})$ is the exciton-plasmon energy given in dimensionless variables $x_\mu = \hbar\omega_\mu/2\gamma_0$ by Eq. (6), which is the solution to the dispersion relation (1) resulted from the diagonalization (see Ref. [29]). The partition function $Q = \text{Tr}(e^{-\beta\hat{H}})$, where $\beta = 1/k_B T$. The chemical potential of the exciton-plasmons is zero as consistent with the fact of no mass added to our system by either exciton or plasmon excitation.

The partition function in Eq. (A1) can be easily evaluated using the exciton-plasmon occupation number Hilbert space vector set $\prod_{\mu=1}^{2} \prod_{\mathbf{k}} |n_\mu(\mathbf{k})\rangle$, resulting in

$$Q = \prod_{\mu=1}^{2} \prod_{\mathbf{k}} \frac{1}{1 - e^{-\beta\hbar\omega_\mu(\mathbf{k})}}. \qquad (A2)$$

Equation (A1) can be evaluated in the same manner, using this partition function, to bring us to the massless boson type exciton-plasmon occupation number

$$\langle n_\mu(\mathbf{k})\rangle = \frac{1}{e^{\beta\hbar\omega_\mu(\mathbf{k})} - 1} = \frac{1}{e^{\lambda x_\mu(\mathbf{k})} - 1}, \qquad (A3)$$

with $\lambda = 2\gamma_0\beta$.

To correctly evaluate the mean population fraction for zero-momentum ($k_z = 0$) exciton-plasmons of the upper branch ($\mu = 1$), we follow the conventional procedure of textbook statistical physics (see, e.g., Refs. [47,65]). We begin with the calculation of the upper-branch exciton-plasmon mean population in the first Brillouin zone. The first Brillouin zone of the carbon nanotube of (m,n) type ($n \leqslant m$) is taken to be consisting of m parallel lines, as per quantized $k_\varphi = k_\varphi(s) = s/R_{CN}$, with $s = 1, 2, \ldots, m$ and $R_{CN} = (\sqrt{3}\,b/2\pi)\sqrt{m^2 + mn + n^2}$ ($b = 1.42$ Å being the C-C distance), each of length $2\tilde{k}_z = 2B/k_\varphi(m)$, where $2B = 2(4\pi^2/3\sqrt{3}\,b^2) = (2\pi)^2/2S_0$ is the rectangular area of the reciprocal space covered by the lines and S_0 is the equilateral triangle area selected around each C atom in such a way as to cover the entire CN surface [12,29]. This yields $\tilde{k}_z = 2\pi/3b$ for the $(m,0)$ type CNs (zigzag) and $\tilde{k}_z = 2\pi/\sqrt{3}\,b$ for the (m,m) type CNs (armchair), in particular. Since the total number of states in the first Brillouin zone is $N/2$ (two C atoms per elementary cell of a graphene layer of N atoms to form a single wall CN of length L, that is $N = 2\pi R_{CN}L/S_0$), the mean population n_1 for the upper-branch exciton-plasmons is

$$n_1 = \frac{2}{N} \sum_{s=1}^{m} \sum_{k_z=-\tilde{k}_z}^{\tilde{k}_z} \langle n_1(s,k_z)\rangle = \frac{2}{N} \sum_{s=1}^{m} \frac{L}{\pi} \int_0^{\tilde{k}_z} dk_z \, \langle n_1(s,k_z)\rangle,$$

where the fact that $\langle n_1(s, -k_z)\rangle = \langle n_1(s,k_z)\rangle$ is taken into account. This can now be rewritten in dimensionless variables to take the form

$$n_1 = \frac{1}{m} \sum_{s=1}^{m} \int_0^1 \frac{dt}{e^{\lambda x_1(s,t)} - 1}, \qquad (A4)$$

with $t = k_z/\tilde{k}_z$ and $x_1(s,t)$, the upper-branch exciton-plasmon energy, to be taken in the form of the expansion of Eq. (6) near $t_c(F) = 0$ under the strong exciton-plasmon coupling condition (controlled by the external perpendicular electrostatic field F by means of the QCSE). Under this condition, $\varepsilon_f \sim x_p$ [avoided crossing in Fig. 2(b)] and the coupling term (that $\sim X_f$) is

dominant under the square root in Eq. (6), to result in the expansion as follows:

$$x_1(F,s,t) \approx X_f(F,s) + \frac{\alpha(s)}{2} t^2, \qquad (A5)$$

with $\alpha(s) = \hbar^2 \tilde{k}_z^2/[2M_{ex}(s)2\gamma_0]$ and the energy counted from $x_2(F,s,t=0)$.

The integral over t in Eq. (A4) can be done by the (geometric) series expansion with subsequent term-by-term integration. Under the assumption of $M_{ex}(s) \approx M_{ex}$ and $X_f(F,s) \approx X(F)$, where M_{ex} and $X(F)$ are those for the first bright exciton in its ground internal state, this results in

$$n_1 = \frac{\sqrt{\pi}}{2} \sum_{n=0}^{+\infty} \frac{e^{-(n+1)\lambda X} \, \text{Erf}[\sqrt{(n+1)\lambda\alpha/2}\,]}{\sqrt{(n+1)\lambda\alpha/2}}. \qquad (A6)$$

Although this model assumption might seem to be questionable from the theoretical viewpoint, the experiment can be set up in such a way as to maintain the system to be continuously illuminated at the first exciton excitation energy. That would correspond to no summation over s and no $1/m$ statistical factor present in the initial Eq. (A4), since only the first exciton would be there contributing to the entire effect with the statistical factor of one. This brings us back to Eq. (A6) again.

The series in Eq. (A6) is seen to converge due to the presence of the exponential factor decaying at a rate that depends on F and T as the summation index n increases. By d'Alembert ratio test the series is convergent absolutely and uniformly when $\exp(-\lambda X) < 1$. This is always the case at finite T $(= 2\gamma_0/k_B\lambda)$ for nonzero X $[= X(F)]$, and the greater is X, the faster is the convergence. The less is X, on the other hand, the slower is the convergence, yielding eventually $\exp(-\lambda X) \sim 1$ at $X \sim 0$ corresponding to divergent harmonic type series typical of 1D and 2D geometries where no BEC phenomenon is known to occur in ideal boson gas type systems [47,67,68]. The quantity $\exp(\lambda X)$ represents the radius of convergence (to be greater than one). This allows us to single out a range of parameters F and T at which the convergence occurs. Setting up $T_c(F) = 2\gamma_0 X(F)/k_B$ yields F such that $\exp(\lambda X) = \exp[T_c(F)/T] > 1$ for all $T \leqslant T_c(F)$, so that the series is manifestly convergent.

For $T \leqslant T_c(F)$ the sum in Eq. (A6) can be evaluated using an approximate expression

$$\sum_{n=0}^{\infty} F(n+a) \approx \int_0^{\infty} dx \, F(x) - F(a)\left(a - \frac{1}{2}\right) + \frac{F'(a)}{2}\left(a^2 - \frac{1}{6}\right) \qquad (A7)$$

that comes from the Euler-Maclaurin summation formula (see Ref. [65])

$$\frac{F(a)}{2} + \sum_{n=1}^{\infty} F(n+a) \approx \int_a^{\infty} dx \, F(x) - \frac{F'(a)}{12}$$

after rearranging the first two terms of the series on the left, writing $\int_a^{\infty} = \int_0^{\infty} - \int_0^a$ on the right and then using a fully legitimate approximation $F(x) \approx F(a) + F'(a)(x - a)$ in the second integral. With $F(n+a) = F(n+1)$, as per Eq. (A6),

this brings us to the following result:

$$n_1 \approx \frac{\arctan(\sqrt{\alpha/2X})}{\lambda\sqrt{\alpha X/2}} + O(e^{-\lambda X}). \qquad (A8)$$

Estimating the argument of the arctangent here, we have

$$\sqrt{\frac{\alpha}{2X}} = \sqrt{\frac{\hbar^2 \tilde{k}_z^2}{4M_{ex}2\gamma_0 X}} = \frac{\pi w}{3}\sqrt{\frac{\hbar^2}{M_{ex}b^2}}\frac{1}{\sqrt{2\gamma_0 X}} \gtrsim 4 \quad (A9)$$

for all reasonable $X \lesssim 0.1$ eV$/2\gamma_0$. We use $\tilde{k}_z = 2\pi w/3b$ with $1 \leqslant w \leqslant \sqrt{3}$ to cover all possible CN chiralities, and M_{ex} is taken to be twice the free electron mass. Thus, Eq. (A8) can be further approximated using the large argument expansion for the arctangent ($\sim \pi/2$), to result in $n_1 \approx \pi/(2\lambda\sqrt{\alpha X/2})$ (exponential smallness neglected), yielding the maximum mean population for the upper-branch exciton plasmons as follows:

$$n_1(T_c) \approx \frac{3}{2w}\sqrt{\frac{M_{ex}b^2}{\hbar^2}}\sqrt{k_B T_c(F)}. \qquad (A10)$$

Next, using Eq. (A3), we proceed to calculate the mean population Δn_1 of the upper-branch exciton-plasmons with $k_z \neq 0$. We have

$$\Delta n_1 = \frac{2}{N}\sum_{s=1}^{m}\left[\sum_{k_z=-\tilde{k}_z}^{-2\pi/L}\langle n_1(s,k_z)\rangle + \sum_{k_z=2\pi/L}^{\tilde{k}_z}\langle n_1(s,k_z)\rangle\right]$$

$$= \frac{2}{N}\sum_{s=1}^{m}\frac{L}{\pi}\int_{2\pi/L}^{\tilde{k}_z}dk_z\,\langle n_1(s,k_z)\rangle = \frac{1}{m}\sum_{s=1}^{m}\int_{t_0}^{1}\frac{dt}{e^{\lambda x_1(s,t)}-1},$$

where $t_0 = 2\pi/L\tilde{k}_z = 4m/N$. After using the (geometric) series expansion followed by term-by-term integration, we arrive at

$$\Delta n_1 = \frac{\sqrt{\pi}}{2}\sum_{n=0}^{+\infty}\frac{e^{-(n+1)\lambda X}}{\sqrt{(n+1)\lambda\alpha/2}}$$

$$\times \{\mathrm{Erf}[\sqrt{(n+1)\lambda\alpha/2}\,] - \mathrm{Erf}[t_0\sqrt{(n+1)\lambda\alpha/2}\,]\}. \qquad (A11)$$

This, after using Eq. (A7) to sum up the series, results in

$$\Delta n_1 \approx \frac{1}{\lambda\sqrt{\alpha X/2}}[\arctan(\sqrt{\alpha/2X}) - \arctan(t_0\sqrt{\alpha/2X})]$$

$$+ O(e^{-\lambda X}). \qquad (A12)$$

Here the estimate for the first term argument is given by Eq. (A9). The second term argument is then $\sim t_0 \sim 1/N$, so that $\arctan(t_0\sqrt{\alpha/2X}) \sim 0$ is negligible. Neglecting also exponentially small terms, as we do in Eq. (A10), brings Eq. (A12) to the following form:

$$\Delta n_1(T,F) \approx \frac{3}{2w}\sqrt{\frac{M_{ex}b^2}{\hbar^2}}\frac{k_B T}{\sqrt{k_B T_c(F)}}. \qquad (A13)$$

Finally, using Eqs. (A10) and (A13), we obtain the (BEC) fraction of zero-momentum exciton-plasmons at $T \leqslant T_c(F)$, defined as

$$\langle n_{10}\rangle(T \leqslant T_c, F) = \frac{n_1(T_c) - \Delta n_1(T,F)}{n_1(T_c)},$$

in the form as given by Eq. (7).

APPENDIX B: DERIVATION OF EQ. (8)

General theory of the exciton-plasmon interactions in individual CNs (see Ref. [29]) relates the operators $\hat{\xi}_\mu^\dagger(\mathbf{k})$ and $\hat{\xi}_\mu(\mathbf{k})$ that create and annihilate, respectively, exciton-plasmons of branch $\mu\,(=1,2)$ with the momentum $\mathbf{k}$, to the exciton creation-annihilation operators $B_{\mathbf{k},f}^\dagger$, $B_{\mathbf{k},f}$ [f-internal state with the energy $E_f(\mathbf{k})$ used in Eqs. (1) and (6)] and the plasmon creation-annihilation operators $\hat{f}^\dagger(\mathbf{k},\omega)$, $\hat{f}(\mathbf{k},\omega)$ as follows:

$$\hat{\xi}_\mu^\dagger(\mathbf{k}) = \sum_f \left[u_{\mu f}^{(\mathrm{ex})}B_{\mathbf{k},f}^\dagger - v_{\mu f}^{*(\mathrm{ex})}B_{-\mathbf{k},f}\right] \qquad (B1)$$

$$+ \int_0^\infty d\omega\left[u_\mu^{*(p)}(\omega)\hat{f}^\dagger(\mathbf{k},\omega) - v_\mu^{(p)}(\omega)\hat{f}(-\mathbf{k},\omega)\right],$$

$$\hat{\xi}_\mu(\mathbf{k}) = [\hat{\xi}_\mu^\dagger(\mathbf{k})]^\dagger.$$

Here $u_{\mu f}^{(\mathrm{ex})}$, $v_{\mu f}^{*(\mathrm{ex})}$, $u_\mu^{*(p)}$, and $v_\mu^{(p)}$ are the complex mixing coefficients that define the (Bogoliubov) unitary canonical transformation on the total Hamiltonian of the coupled exciton-plasmon system to bring it to the diagonal form [used in Eq. (A1)]. These mixing coefficients are given by the solutions to the following set of simultaneous linear equations:

$$(\hbar\omega_\mu - E_f)u_{\mu f}^{(\mathrm{ex})} = i\int_0^\infty d\omega D_f(\omega)\left[u_\mu^{*(p)}(\omega) - v_\mu^{(p)}(\omega)\right],$$
$$(B2)$$

$$(\hbar\omega_\mu + E_f)v_{\mu f}^{*(\mathrm{ex})} = -i\int_0^\infty d\omega D_f(\omega)\left[u_\mu^{*(p)}(\omega) - v_\mu^{(p)}(\omega)\right],$$
$$(B3)$$

$$\hbar(\omega_\mu - \omega)u_\mu^{*(p)}(\omega) = -i\sum_f D_f(\omega)\left[u_{\mu f}^{(\mathrm{ex})} + v_{\mu f}^{*(\mathrm{ex})}\right], \quad (B4)$$

$$\hbar(\omega_\mu + \omega)v_\mu^{(p)}(\omega) = -i\sum_f D_f(\omega)\left[u_{\mu f}^{(\mathrm{ex})} + v_{\mu f}^{*(\mathrm{ex})}\right], \quad (B5)$$

where $D_f(\omega) = \hbar\sqrt{\Gamma_0^f(\omega)\rho(\omega)/2\pi}$ is the exciton-plasmon interaction matrix element with $\Gamma_0^f(\omega)$ and $\rho(\omega)$ representing the frequency dependencies of the exciton spontaneous decay rate and that of the plasmon DOS function responsible for the exciton decay rate variation due to its (nonradiative) coupling to CN plasmon modes [given in dimensionless variables by Eqs. (4) and (5), respectively].

Equations (B2)–(B5) define the mixing coefficients, as well as they define the dispersion relation for the exciton-plasmon energy $\hbar\omega_\mu(\mathbf{k})$ that is used in Eqs. (A1)–(A3) and (in the dimensionless form) in Eqs. (6) and (A5). The dispersion relation is given by Eq. (1), and the details of its derivation can be found in Ref. [29]. Here we solve the set of Eqs. (B2)–(B5) for the mixing coefficients.

We are particularly interested in finding the coefficients $u_{\mu f}^{(\mathrm{ex})}$ and $u_\mu^{*(p)}(\omega)$ since, as we can see from Eq. (B1), the absolute value squared of their ratio shows the exciton participation against the plasmon participation in an exciton-plasmon

excitation created. Combining Eqs. (B2) and (B3) yields

$$v_{\mu f}^{*(\mathrm{ex})} = \frac{E_f - \hbar\omega_\mu}{E_f + \hbar\omega_\mu} u_{\mu f}^{(\mathrm{ex})}, \tag{B6}$$

while from Eqs. (B4) and (B5) we have

$$v_\mu^{(p)}(\omega) = \frac{\omega_\mu - \omega}{\omega_\mu + \omega} u_\mu^{*(p)}(\omega). \tag{B7}$$

Next, from Eq. (B4), using Eq. (B6) in its right-hand side, one obtains

$$u_\mu^{*(p)}(\omega) = i \sum_f \frac{2 E_f D_f(\omega)}{\hbar(\omega - \omega_\mu)(E_f + \hbar\omega_\mu)} u_{\mu f}^{(\mathrm{ex})}, \tag{B8}$$

which being substituted into Eq. (B7) results in

$$v_\mu^{(p)}(\omega) = -i \sum_f \frac{2 E_f D_f(\omega)}{\hbar(\omega + \omega_\mu)(E_f + \hbar\omega_\mu)} u_{\mu f}^{(\mathrm{ex})}. \tag{B9}$$

Equations (B6), (B8), and (B9), with $u_{\mu f}^{(\mathrm{ex})}$ determined by the normalization condition, solve the equations set (B2)–(B5). They can be written in the dimensionless variables (2) used throughout this paper as follows:

$$v_{\mu f}^{*(\mathrm{ex})} = \frac{\varepsilon_f - x_\mu}{\varepsilon_f + x_\mu} u_{\mu f}^{(\mathrm{ex})}, \tag{B10}$$

$$\bar{u}_\mu^{*(p)}(x) = i \sum_f \frac{2\,\varepsilon_f \sqrt{\bar{\Gamma}_0^f(x)\rho(x)/2\pi}}{(x - x_\mu)(\varepsilon_f + x_\mu)} u_{\mu f}^{(\mathrm{ex})}, \tag{B11}$$

$$\bar{v}_\mu^{(p)}(x) = -i \sum_f \frac{2\,\varepsilon_f \sqrt{\bar{\Gamma}_0^f(x)\rho(x)/2\pi}}{(x + x_\mu)(\varepsilon_f + x_\mu)} u_{\mu f}^{(\mathrm{ex})}, \tag{B12}$$

where $\bar{u}_\mu^{*(p)} = u_\mu^{*(p)}\sqrt{2\gamma_0/\hbar}$ and $\bar{v}_\mu^{(p)} = v_\mu^{(p)}\sqrt{2\gamma_0/\hbar}$ are the dimensionless counterparts of the corresponding mixing coefficients. Assuming further that the ground internal state of the exciton contributes the most to the summations over f in the expressions above, we arrive at the ratio of interest in the form (f subscript dropped)

$$\frac{\left|u_\mu^{(\mathrm{ex})}\right|^2}{\left|\bar{u}_\mu^{*(p)}\right|^2} \approx \frac{\pi(x - x_\mu)^2(1 + x_\mu/\varepsilon)^2}{2\bar{\Gamma}_0(x)\rho(x)}. \tag{B13}$$

To obtain the exciton participation rate in the upper-branch ($\mu = 1$) exciton-plasmon BEC population fraction, we

note that the denominator in Eq. (B13) is nothing but the (dimensionless) exciton-plasmon interaction matrix element squared. This is only nonzero when the exciton energy $\varepsilon = \varepsilon(F,t)$ and the plasmon resonance energy $x_p(F)$ are close in their values. As this takes place, the plasmon DOS $\rho(x)$ can be legitimately approximated by the Lorentzian of the half-width at half-maximum Δx_p (representing the inverse plasmon lifetime) of the form

$$\rho(x) \approx \frac{\rho(x_p)\Delta x_p^2}{(x - x_p)^2 + \Delta x_p^2},$$

in which the frequency x is equal to $\varepsilon(F,t)$ and this latter one is assumed to be of the order of $x_p(F)$. With this in mind, we write the denominator in Eq. (B13) as follows:

$$2\bar{\Gamma}_0(x)\rho(x) = 2\bar{\Gamma}_0[\varepsilon(F,t)]\rho[\varepsilon(F,t)] = \frac{X^2(F,t)}{\Delta x_p}.$$

Then, Eq. (B13) for the upper-branch exciton-plasmons takes the form

$$\frac{\left|u_1^{(\mathrm{ex})}\right|^2}{\left|\bar{u}_1^{*(p)}\right|^2} \approx \frac{\pi\,\Delta x_p(x - x_1)^2[1 + x_1/\varepsilon(F,t)]^2}{X^2(F,t)}, \tag{B14}$$

where the energies should be counted from $x_2(F,t=0)$ as per our previous convention.

Figure 3(a) shows functions $2\gamma_0 X(F,t)/k_B\ [= T_c(F,t)]$ we calculated for the lowest bright ground-internal-state excitons coupled to the nearest interband plasmons in the four CNs of our choice here. Function $X(F,t)$ is sharp resonance shaped with the peak position determined by the condition $\varepsilon(F,t) = x_p(F)$ [cf. Fig. 2(b)]. As F increases, the peak shifts down to $t \sim 0$, yielding $X(F) = X(F,t=0)$ sharply peaked around $F = F_c$. This suggests that, when at resonance, the ratio (B14) is generally much less than one, so that exciton-plasmon excitations are dominated by plasmons. However, a slight detuning from the resonance condition decreases $X^2(F,t)$ dramatically, making the ratio (B14) dramatically increase and excitons dominate an exciton-plasmon state.

Using Eq. (B14), the exciton participation rate in the exciton-plasmon BEC population fraction can be found as follows:

$$\langle n_{10}\rangle_{E/P}(x,T,F) = \left.\frac{\left|u_1^{(\mathrm{ex})}\right|^2}{\left|\bar{u}_1^{*(p)}\right|^2}\right|_{t=0} \langle n_{10}\rangle(T \leqslant T_c,F),$$

which brings us to Eq. (8).

[1] M. Dresselhaus, G. Dresselhaus, and Ph. Avouris (eds.), *Carbon Nanotubes: Synthesis, Structure, Properties, and Applications* (Springer, Berlin, 2001).

[2] M. F. L. De Volder, S. H. Tawfick, R. H. Baughman, and A. J. Hart, Science **339**, 535 (2013).

[3] T. Hertel and I. V. Bondarev, Chem. Phys. **413**, 1 (2013).

[4] M. S. Dresselhaus, G. Dresselhaus, R. Saito, and A. Jorio, Annu. Rev. Phys. Chem. **58**, 719 (2007).

[5] Ph. Avouris, M. Freitag, and V. Perebeinos, Nat. Photon. **2**, 341 (2008).

[6] F. Vietmeyer, B. Seger, and P. V. Kamat, Adv. Mater. **19**, 2935 (2007).

[7] N. M. Gabor, Z. Zhong, K. Bosnick, J. Park, and P. L. McEuen, Science **325**, 1367 (2009).

[8] T. Hertel, Nat. Photon. **4**, 77 (2010).

[9] T. Mueller, M. Kinoshita, M. Steiner, V. Perebeinos, A. A. Bol, D. B. Farmer, and Ph. Avouris, Nat. Nanotech. **5**, 27 (2010).

[10] X. Dang, H. Yi, M.-H. Ham, J. Qi, D. S. Yun, R. Ladewski, M. S. Strano, P. T. Hammond, and A. M. Belcher, Nat. Nanotechnol. **6**, 377 (2011).

[11] E. Malic, C. Weber, M. Richter, V. Atalla, T. Klamroth, P. Saalfrank, S. Reich, and A. Knorr, Phys. Rev. Lett. **106**, 097401 (2011).

[12] I. V. Bondarev, Phys. Rev. B **85**, 035448 (2012).

[13] I. V. Bondarev and T. Antonijevic, Phys. Status Solidi C **9**, 1259 (2012).

[14] S. Nanot, E. H. Haroz, J.-H. Kim, R. H. Hauge, and J. Kono, Adv. Mater. **24**, 4977 (2012).

[15] A. Hagen, M. Steiner, M. B. Raschke, C. Lienau, T. Hertel, H. Qian, A. J. Meixner, and A. Hartschuh, Phys. Rev. Lett. **95**, 197401 (2005).

[16] B. F. Habenicht and O. V. Prezhdo, Phys. Rev. Lett. **100**, 197402 (2008).

[17] B. O. Tayo and S. V. Rotkin, Phys. Rev. B **86**, 125431 (2012).

[18] F. Plentz, H. B. Ribeiro, A. Jorio, M. S. Strano, and M. A. Pimenta, Phys. Rev. Lett. **95**, 247401 (2005).

[19] V. Perebeinos, J. Tersoff, and Ph. Avouris, Phys. Rev. Lett. **94**, 027402 (2005).

[20] S. Piscanec, M. Lazzeri, J. Robertson, A. C. Ferrari, and F. Mauri, Phys. Rev. B **75**, 035427 (2007).

[21] T. G. Pedersen, K. Pedersen, H. D. Cornean, and P. Duclos, Nano Lett. **5**, 291 (2005).

[22] D. Kammerlander, D. Prezzi, G. Goldoni, E. Molinari, and U. Hohenester, Phys. Rev. Lett. **99**, 126806 (2007).

[23] I. V. Bondarev, Phys. Rev. B **83**, 153409 (2011).

[24] R. Matsunaga, K. Matsuda, and Y. Kanemitsu, Phys. Rev. Lett. **106**, 037404 (2011).

[25] K. Watanabe and K. Asano, Phys. Rev. B **85**, 035416 (2012).

[26] T. F. Ronnow, T. G. Pedersen, and B. Partoens, Phys. Rev. B **85**, 045412 (2012).

[27] L. Colombier, J. Selles, E. Rousseau, J. S. Lauret, F. Vialla, C. Voisin, and G. Cassabois, Phys. Rev. Lett. **109**, 197402 (2012).

[28] B. Yuma, S. Berciaud, J. Besbas, J. Shaver, S. Santos, S. Ghosh, R. B. Weisman, L. Cognet, M. Gallart, M. Ziegler, B. Hönerlage, B. Lounis, and P. Gilliot, Phys. Rev. B **87**, 205412 (2013).

[29] I. V. Bondarev, L. M. Woods, and K. Tatur, Phys. Rev. B **80**, 085407 (2009); Opt. Commun. **282**, 661 (2009).

[30] A. Srivastava, H. Htoon, V. I. Klimov, and J. Kono, Phys. Rev. Lett. **101**, 087402 (2008).

[31] V. Perebeinos and Ph. Avouris, Nano Lett. **7**, 609 (2007).

[32] C. W. Chang, D. Okawa, A. Majumdar, and A. Zettl, Science **314**, 1121 (2006).

[33] E. Cobas and M. Fuhrer, Appl. Phys. Lett. **93**, 043120 (2008).

[34] P. Myllyperkio, O. Herranen, J. Rintala, H. Jiang, P. R. Mudimela, Z. Zhu, A. G. Nasibulin, A. Johansson, E. I. Kauppinen, M. Ahlskog, and M. Pettersson, ACS Nano **4**, 6781 (2011).

[35] F. Xia, M. Steiner, Y.-M. Lin, and Ph. Avouris, Nat. Nanotechnol. **3**, 609 (2008).

[36] A. Högele, C. Galland, M. Winger, and A. Imamoglu, Phys. Rev. Lett. **100**, 217401 (2008).

[37] I. V. Bondarev, J. Comp. Theor. Nanosci. **7**, 1673 (2010); J. Electron. Mater. **36**, 1579 (2007).

[38] C. D. Spataru, S. Ismail-Beigi, R. B. Capaz, and S. G. Louie, Phys. Rev. Lett. **95**, 247402 (2005).

[39] C. D. Spataru and F. Léonard, Phys. Rev. Lett. **104**, 177402 (2010).

[40] Y. Zhang, T.-T. Tang, C. Girit, Z. Hao, M. C. Martin, A. Zettl, M. F. Crommie, Y. Ron Shen, and F. Wang, Nature (London) **459**, 820 (2009).

[41] I. V. Bondarev, Phys. Status Solidi B **248**, 468 (2011); Superlattices Microstruct. **49**, 217 (2011).

[42] Electrostatic fields reported earlier for the QCSE on CNs must be multiplied by the factor $1/\sqrt{4\pi\epsilon_0}$ to result in field strengths ~ 1 V/nm, consistent with the fields observed for the QCSE on bilayer graphene [40]. I.V.B. is indebted to Dr. A. Högele of LMU, Germany, for bringing this issue to his attention.

[43] P. Y. Yu and M. Cardona, *Fundamentals of Semiconductors* (Springer, Heidelberg, 2010).

[44] Y. Toyozawa, *Optical Processes in Solids* (Cambridge University Press, Cambridge, 2003).

[45] T. Ando, J. Phys. Soc. Jpn. **74**, 777 (2005).

[46] D. J. Bergman and M. I. Stockman, Phys. Rev. Lett. **90**, 027402 (2003).

[47] R. P. Feynman, *Statistical Mechanics* (W. A. Benjamin, Reading, MA, 1972).

[48] Y. Murakami and J. Kono, Phys. Rev. Lett. **102**, 037401 (2009).

[49] V. Bagnato and D. Kleppner, Phys. Rev. A **44**, 7439 (1991); W.-S. Dai and M. Xie, *ibid.* **67**, 027601 (2003).

[50] M. I. Stockman, Phys. Today **64**(2), 39 (2011).

[51] L. Novotny, Phys. Today **64**(7), 47 (2011).

[52] L. D. Landau and E. M. Lifshits, *The Classical Theory of Fields* (Pergamon, New York, 1975).

[53] T. Pichler, M. Knupfer, M. S. Golden, J. Fink, A. Rinzler, and R. E. Smalley, Phys. Rev. Lett. **80**, 4729 (1998).

[54] K. Kempa and R. Chura, in *Low-Dimensional Systems: Theory, Preparation, and Some Applications*, edited by L. M. Liz-Marzan and M. Giersig, NATO Science Book Series (Kluwer, Dordrecht, 2003), Vol. 91, pp. 37–43.

[55] K. Kempa, D. A. Broido, C. Beckwith, and J. Cen, Phys. Rev. B **40**, 8385 (1989).

[56] Y.-Z. Ma, C. D. Spataru, L. Valkunas, S. G. Louie, and G. R. Fleming, Phys. Rev. B **74**, 085402 (2006).

[57] L. X. Benedict, S. G. Louie, and M. L. Cohen, Phys. Rev. B **52**, 8541 (1995).

[58] S. Tasaki, K. Maekawa, and T. Yamabe, Phys. Rev. B **57**, 9301 (1998).

[59] A. G. Marinopoulos, L. Reining, A. Rubio, and N. Vast, Phys. Rev. Lett. **91**, 046402 (2003).

[60] B. Kozinsky and N. Marzari, Phys. Rev. Lett. **96**, 166801 (2006).

[61] Z. M. Li, Z. K. Tang, H. J. Liu, N. Wang, C. T. Chan, R. Saito, S. Okada, G. D. Li, J. S. Chen, N. Nagasawa, and S. Tsuda, Phys. Rev. Lett. **87**, 127401 (2001).

[62] I. V. Bondarev and Ph. Lambin, Phys. Rev. B **70**, 035407 (2004).

[63] I. V. Bondarev and Ph. Lambin, Phys. Rev. B **72**, 035451 (2005).

[64] I. V. Bondarev and Ph. Lambin, *Trends in Nanotubes Research* (Nova Science, New York, 2006), Chap. 6, pp. 139–183.

[65] L. D. Landau and E. M. Lifshitz, *Statistical Physics* (Pergamon, Oxford, 1980).

[66] T. Ando, J. Phys. Soc. Jpn. **75**, 024707 (2006).

[67] P. C. Hohenberg, Phys. Rev. **158**, 383 (1967).

[68] L. Pitaevskii and S. Stringari, *Bose-Einstein Condensation* (Clarendon, Oxford, 2003).

[69] J. Kasprzak, M. Richard, S. Kundermann, A. Baas, P. Jeambrun, J. M. J. Keeling, F. M. Marchetti, M. H. Szymanska, R. Andre, J. L. Staehli, V. Savona, P. B. Littlewood, B. Deveaud, and L. S. Dang, Nature (London) **443**, 409 (2006).

[70] A. Kavokin, Appl. Phys. A **89**, 241 (2007).